REPORT

Recurrent De Novo Mutations in *PACS1* Cause Defective Cranial-Neural-Crest Migration and Define a Recognizable Intellectual-Disability Syndrome

Janneke H.M. Schuurs-Hoeijmakers,[1,8] Edwin C. Oh,[2,8] Lisenka E.L.M. Vissers,[1,8] Mariëlle E.M. Swinkels,[3] Christian Gilissen,[1] Michèl A. Willemsen,[4,5] Maureen Holvoet,[6] Marloes Steehouwer,[1] Joris A. Veltman,[1] Bert B.A. de Vries,[1,5] Hans van Bokhoven,[1,5] Arjan P.M. de Brouwer,[1,5] Nicholas Katsanis,[2,7,9] Koenraad Devriendt,[6,9] and Han G. Brunner[1,9,*]

We studied two unrelated boys with intellectual disability (ID) and a striking facial resemblance suggestive of a hitherto unappreciated syndrome. Exome sequencing in both families identified identical de novo mutations in *PACS1*, suggestive of causality. To support these genetic findings and to understand the pathomechanism of the mutation, we studied the protein in vitro and in vivo. Altered PACS1 forms cytoplasmic aggregates in vitro with concomitant increased protein stability and shows impaired binding to an isoform-specific variant of TRPV4, but not the full-length protein. Furthermore, consistent with the human pathology, expression of mutant *PACS1* mRNA in zebrafish embryos induces craniofacial defects most likely in a dominant-negative fashion. This phenotype is driven by aberrant specification and migration of SOX10-positive cranial, but not enteric, neural-crest cells. Our findings suggest that PACS1 is necessary for the formation of craniofacial structures and that perturbation of its functions results in a specific syndromic ID phenotype.

Intellectual disability (ID) affects 1%–3% of the population and has a strong genetic component. Despite technical progress, establishing a genetic diagnosis remains challenging, in part because of substantial genetic heterogeneity and clinical variability.[1] Recent data have indicated a high rate of de novo events in ID,[2] suggesting that family-based exome sequencing can be an efficient tool for identifying genetic causes of ID and thus for probing its molecular etiology.

We recruited two unrelated boys with unexplained ID and a remarkable facial resemblance (Figure 1A). This study was approved by the Medical Ethics Committee of the Radboud University Nijmegen Medical Centre, and all participants signed informed consent. The first boy (individual 1) is the only child of unrelated Dutch parents. A paternal cousin of individual 1 also has developmental delay, but it is of a different severity and physical appearance. He was therefore considered to have an unrelated clinical condition. Individual 1 was born at term by vacuum extraction after an uncomplicated pregnancy. The mother was treated with mesalazine for Crohn disease throughout the pregnancy. His birth weight was 3,250 g (25^{th} percentile), and his Apgar (appearance, pulse, grimace, activity, respiration) score was 5, 6, and 8 at 1, 5, and 10 minutes, respectively. A single umbilical artery was noted. On the second day of life, he developed seizures, which were successfully treated with antiepileptic medication. Four weeks after birth, the boy developed volvulus by intestinal malrotation. Resection of a large part of the small intestine was performed upon emergency laparatomy. He developed short-bowel syndrome, for which he received total parenteral feeding until age 4 years, and was tube fed thereafter. A vesicourethral reflux grade II resolved spontaneously. Left-sided cryptorchidism was surgically corrected by orchidopexy. During this operation, a streak testis was observed on the right side. Development was delayed: he was able to sit with support at age 10 months, walked at age 3 years and 4 months, and spoke his first words at age 3 years and 6 months. Language production was more delayed than verbal understanding, and dyspraxia was noted. His intelligence quotient (IQ) was measured as <50. On physical examination, we saw a friendly boy with some stereotypic movements. When he was 3 years and 6 months old, his weight was 15 kg (16^{th} percentile), his length was 102 cm (50^{th} percentile), and his orbitofrontal cortex (OFC) was 49 cm (16^{th} percentile). His facial features were characterized by a low anterior hairline, hypertelorism with downslanting palpebral fissures, mild synophrys with highly arched eyebrows, long eyelashes, a bulbous nose, a flat philtrum, and large, low-set ears (6 cm [97^{th} percentile]). He has a wide mouth with downturned corners, a thin upper lip, and diastema

[1]Department of Human Genetics 855, Nijmegen Centre for Molecular Life Sciences and Institute for Genetic and Metabolic Disease, Radboud University Nijmegen Medical Centre, PO Box 9101, 6500 HB Nijmegen, The Netherlands; [2]Center for Human Disease Modeling, Duke University, Durham NC 27710, USA; [3]Medical Genetics, University Medical Center Utrecht, 3508 AB Utrecht, The Netherlands; [4]Department of Pediatric Neurology, Radboud University Nijmegen Medical Centre, PO Box 9101, 6500 HB Nijmegen, The Netherlands; [5]Donders Institute for Brain, Cognition, and Behaviour, Radboud University Nijmegen, PO Box 9104, 6500 HE Nijmegen, The Netherlands; [6]Center for Human Genetics, Clinical Genetics, University Hospitals Leuven, Herestraat 49 BUS 602, 3000 Leuven, Belgium; [7]Departments of Cell Biology and Pediatrics, Duke University, Durham NC 27710, USA
[8]These authors contributed equally to this work
[9]These authors contributed equally to this work
*Correspondence: h.brunner@gen.umcn.nl
http://dx.doi.org/10.1016/j.ajhg.2012.10.013.

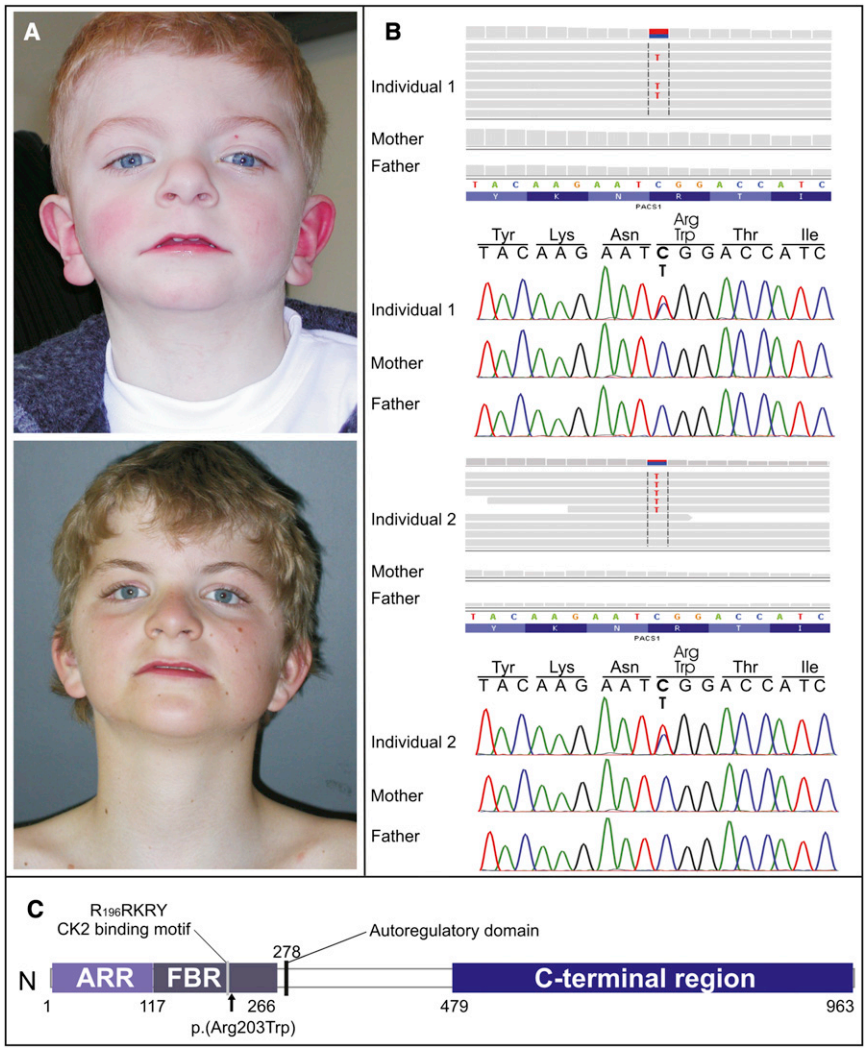

Figure 1. Photographs and Genetic Data of Two Unrelated Individuals with an Identical De Novo Mutation in *PACS1*

(A) Upper photograph: individual 1 at 4 years of age with a low anterior hairline, highly arched eyebrows, synophrys, hypertelorism with downslanted palpebral fissures, long eyelashes, a bulbous nasal tip, a flat philtrum with a thin upper lip, downturned corners of the mouth, diastema of the teeth, and low-set ears. Bottom photograph: individual 2 at 12 years of age. Note the remarkable facial similarity.

(B) Sequence reads from exome sequencing and chromatograms of Sanger confirmation show the identical de novo occurrence of the c.607C>T mutation in *PACS1* (RefSeq NM_018026.2) in individuals 1 and 2.

(C) Protein structure of PACS1. The position of the p.Arg203Trp substitution is indicated in the furin (cargo)-binding region (FBR) of the protein and is directly adjacent to the CK2-binding motif.

of the teeth (Figure 1A). Widely spaced nipples, slender fingers (but broad and short thumbs), clubbed nails, a single transverse palmar crease on the left hand, and pes planus were also noted. Neurological examination showed simple motor patterns without specific pyramidal, extrapyramidal, cerebellar, or neuromuscular abnormalities. Cerebral MRI showed a cavum septum pellucidum but was otherwise normal. Conventional karyotyping, as well as SNP array testing (Affymetrix, 250K), showed a normal male karyotype. Because of some facial similarities to Cornelia de Lange syndrome (MIM 122470), *NIPBL* (MIM 608667), *SMC1A* (MIM 300040), and *SMC3* (MIM 606062) were sequenced for mutations, but none were found.

The second boy (individual 2) is the second child of healthy, unrelated parents of Belgium origin. There was one previous miscarriage. Family history is negative with regard to developmental delay or congenital malformations. The boy was born at term by caesarian section because of breech presentation. His birth weight was 4,250 g (90^{th} percentile), his length was 54 cm (97^{th} percentile), and his OFC was 36 cm (90^{th} percentile). His development was delayed. He walked at the age of 2 years and 6 months. His IQ was measured as 53. Currently, at age 19 years, he functions well in a special school and, except for mild scoliosis, has no medical problems. When first seen at the age of 6 years and 3 months, he appeared friendly and outgoing. His weight was 22 kg (50^{th} percentile), his length was 119 cm (50^{th} percentile), and his OFC was 51.7 cm (50^{th} percentile). When he was seen at 19 years of age, his measurements were a weight of 64.5 kg (16^{th} percentile), a length of 181 cm (50^{th} percentile), and an OFC of 55.1 cm (16^{th} percentile). His facial features were characterized by hypertelorism with downslanting palpebral fissures, strabismus, long eyelashes and mild ectropion, highly arched eyebrows, downturned corners of the mouth, a narrow upper lip (especially in its middle part), and a flat philtrum (Figure 1A). His teeth were widely spaced, and his ears were low set. He had a short neck, widely spaced nipples, and a mild pectus excavatum. He had clinodactyly and shortness of the fifth fingers and mild cutaneous webbing of the fingers. The skin showed multiple pigmented nevi. He had a small umbilical hernia, hypoplastic scrotum, and cryptorchidism on the right side. Neurological examination showed balance problems and mild dysarthric speech. He was hypotonic. A conventional karyotype and array comparative genomic hybridization (Agilent 180K) showed a normal male karyotype. A computed-tomography scan of the brain revealed a partial agenesis of the vermis and hypoplasia of the cerebellar hemispheres, which was more pronounced on the right side.

Because of their striking similar facial dysmorphisms, which were unique among our cohort of >5,000 individuals with ID, we considered this a distinct dominant syndrome with plausibly a common genetic defect. Aiming at the identification of a causal de novo mutation, we therefore performed exome sequencing on DNA from both index-parent trios by using the ABI SOLiD 4 platform (Life Technologies, Carlsbad, CA, USA) (described previously by Vissers et al.[2]) (Table S1, available online). Seven potential de novo nonsynonymous variants were identified in individual 1, and six were identified in individual 2 (Table S2). Sanger validation confirmed two as de novo in individual 1 and one in individual 2. Remarkably, the same de novo c.607C>T mutation in *PACS1* (RefSeq accession number NM_018026.2 [MIM 607492]) was identified in both individuals (Figure 1B). This mutation is predicted to result in an arginine-to-tryptophan substitution, p.Arg203Trp (Figure 1C), at an evolutionarily invariant position in both PACS1 and its close paralog PACS2 (Figure S2). The c.607C>T mutation was absent in 150 alleles of control individuals of the Dutch population, in 2,304 alleles present in our local variant database (which is derived from exome-sequencing experiment), and in 7,020 alleles of European American origin from the National Heart, Lung, and Blood Institute (NHLBI) Exome Sequencing Project.

PACS1 is a trans-golgi-membrane traffic regulator[3,4] that directs protein cargo and several viral-envelope proteins.[4–6] *PACS1* mRNA expression is upregulated during human embryonic brain development and has low expression after birth (see BrainSpan: Atlas of the Developing Human Brain in Web Resources). PACS1 contains a furin (cargo)-binding region (FBR) bearing a CK2-binding motif, an autoregulatory domain, and N- and C-terminal ends of unknown function. Our p.Arg203Trp substitution is positioned in the FBR directly adjacent to the R^{196}RKRY CK2-binding motif that regulates the phosphorylation status of the autoregulatory domain and PACS1 activation[7,8] (Figure 1C).

The chance to observe an identical de novo base-pair change in two individuals is extremely small, indicating that our recurrent finding of the exact same de novo base-pair change in these individuals with identical clinical presentation and its absence from ~9,000 control alleles strongly support causality. However, to provide further evidence and to probe the mechanistic basis of the dysmorphic phenotype, we studied the behavior of the p.Arg203Trp substitution in craniofacial cartilaginous structures in zebrafish embryos. We injected either wild-type (c.607C [p.Arg203]) or mutant (c.607T [p.Trp203]) human *PACS1* mRNA into 2- to 4-cell-stage zebrafish embryos. On scoring Alcian-blue-stained 4-day-old embryos injected with either 50 pg wild-type or 50 pg mutant *PACS1* mRNA ($n = 61$ embryos per batch; scored blind to injection cocktail), we observed that relative to embryos expressing wild-type *PACS1*, embryos expressing mutant *PACS1* showed a significant reduction in cranial cartilaginous structures at the ventral aspect ($p < 0.001$); embryos expressing wild-type *PACS1* were indistinguishable from uninjected control zebrafish (Figure 2A and Figure S4B). The induction of a craniofacial phenotype upon overexpression of mutant human *PACS1* mRNA argues against a loss-of-function effect of the mutation but cannot differentiate between a gain-of-function or dominant-negative mechanism. To examine these possibilities, we injected equimolar ratios of 50 pg wild-type and 50 pg mutant mRNA together. We observed a significant rescue of the mutant craniofacial phenotype ($n = 55$; $p < 0.001$), suggestive of a dominant-negative mechanism (Figure 2A).

The loss of craniofacial structures upon expression of mutant *PACS1* mRNA might be the result of defective migration of cranial-neural-crest cells (CNCCs), progenitors that give rise to the majority of skeletal and connective tissues in the face.[9–11] As an initial test of this hypothesis, we injected wild-type or mutant RNA in 2- to 4-cell-stage sox10::eGFP transgenic zebrafish embryos, which express green fluorescent protein (GFP) in CNCCs. Analysis of 4-day-old embryos showed a significant reduction in the migration of GFP-labeled cells ($n = 55$; $p < 0.001$) in the anterior-most region of the embryo (head), confirming that the absence of Alcian-blue staining is at least in part due to the loss of CNCC-derived progenitors (Figure 2B). To examine the specificity of the CNCC-migration phenotype, we isolated RNA from the trunk and head regions of injected embryos and analyzed sox10::eGFP-positive cells harvested from enteric-neural-crest cells (ENCCs) and CNCCs. We observed a significant reduction in GFP mRNA levels in the head. The phenotype was specific to this region; we observed no differences in GFP mRNA levels in the trunk of injected embryos (Figure S3). Together, these data suggest that PACS1 can promote the specification and migration of CNCCs, although fate-mapping studies will be required for substantiating these observations.

To assess whether the phenotypes observed in the two affected individuals and zebrafish embryos might be the result of misfolding and/or mistrafficking of the protein, we studied GFP-tagged wild-type (p.Arg203) and altered (p.Trp203) PACS1 in ARPE-19 cells. We examined the localization of the constructs in cells grown to confluence. Analysis of ~150 cells showed that 32% of cells with the altered construct contained cytoplasmic GFP aggregates, a phenotype seen in <4% of cells with the wild-type construct (Figure 3A). Because aggregates of the altered GFP-tagged p.Trp203 PACS1 might be the result of misfolding, we next queried whether altered PACS1 stability might also be perturbed. We transfected wild-type and altered PACS1 constructs into human embryonic kidney (HEK) 293FT cells (given that transfection efficiency is >90%). Whereas GFP expression of wild-type PACS1 diminishes over time, expression of altered PACS1 remains constant, indicating that the altered protein remains more stable than the wild-type protein (Figure 3B and Figure S4A).

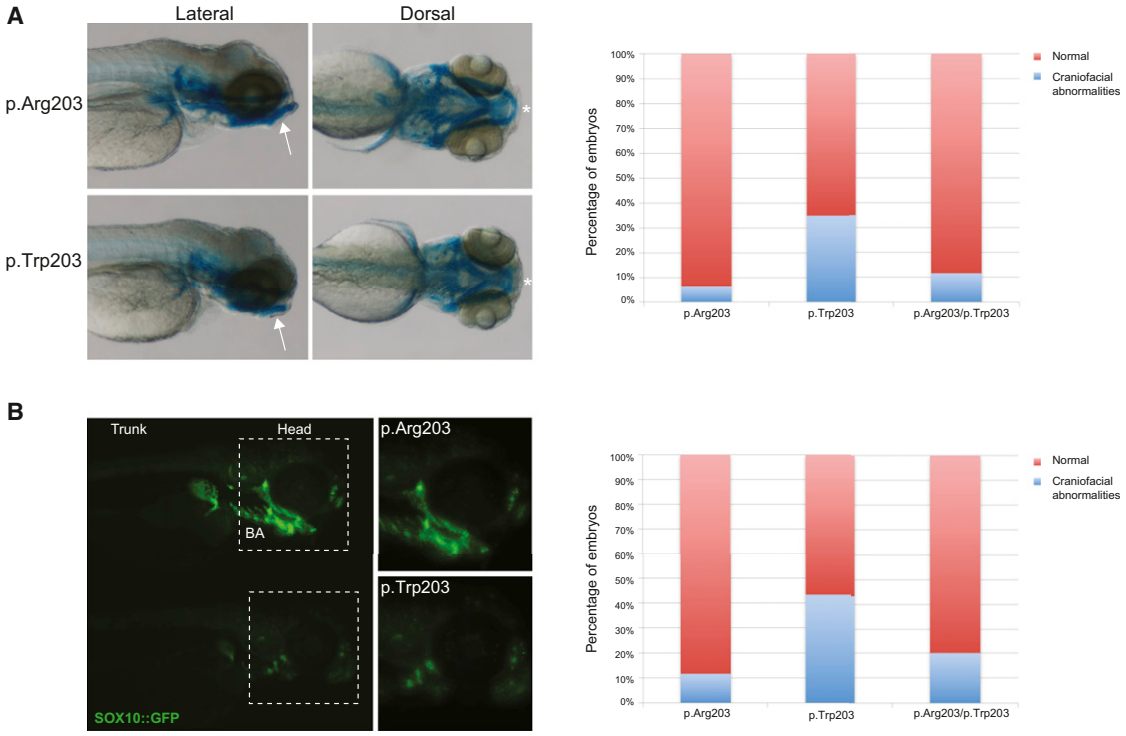

Figure 2. In Vivo Functional Characterization of the p.Arg203Trp Substitution in PACS1
(A) Alcian-blue staining of 4-day-old zebrafish larvae expressing either 50 pg wild-type (c.607C [p.Arg203]) or 50 pg mutant (c.607T [p.Trp203]) *PACS1* RNA. Left panel: craniofacial cartilaginous structures visualized in both lateral and ventral views of the embryo. Right panel: craniofacial phenotypes in embryos expressing wild-type *PACS1*, mutant *PACS1*, and both wild-type and mutant *PACS1* are quantified. White arrows and asterisks highlight Meckel's cartilage in the lateral and ventral perspectives of the embryos. Human wild-type and mutant *PACS1* mRNA was transcribed in vitro with a mMESSAGE mMACHINE SP6 Kit (Ambion), and 0.5 nl was microinjected into 2- to 4-cell-stage zebrafish embryos.
(B) Imaging of 4-day-old sox10::eGFP zebrafish larvae expressing either 50 pg wild-type or mutant *PACS1* RNA. Left panel: migration of eGFP-labeled cranial-neural-crest cells (CNCCs). Right panel: CNCC-migration phenotype scored in embryos expressing wild-type PACS1, altered PACS1, and both wild-type and altered PACS1.

Given that we observed cellular aggregates, as well as defects in protein stability, we next asked whether the altered variant changes the formation of PACS1-dependent complexes. We observed no significant effect of altered PACS1 on two known interactors, AP3D1 and CLCN7 (data not shown). However, we observed a significant phenotype for a third interactor, TRPV4. Specifically, we cotransfected GFP-tagged PACS1 with V5-tagged full-length TRPV4 (TRPV4v1; RefSeq NM_021625) and a smaller TRPV4 (TRPV4v2; RefSeq NM_147204) isoform that is missing residues 311–371, which are predicted to encode an ankyrin repeat. Although both wild-type and altered PACS1 bound to full-length TRPV4 at similar affinities, we detected significantly less TRPV4v2 in the immunoprecipitate with the altered PACS1 (Figure 3C). TPRV4 has been implicated in the migration of tumor endothelial cells,[12] in visceral mechanosensation,[13] and, more broadly, in the F-actin-mediated regulation of the shape of cellular surfaces.[14] It is unclear how TRPV4v2 participates in disease etiology, but we note that impairment of its known role in visceral mechanosensation in the gastrointestinal tract might have contributed to the volvulus that individual 1 experienced in the neonatal period.[13] Furthermore, the binding of full-length TRPV4 to wild-type and altered PACS1 is consistent with the lack of anosmia in individuals 1 and 2.[15–17] Our data suggest that the introduction of the p.Arg203Trp substitution triggers cytoplasmic aggregates, leads to protein-trafficking defects, and most likely abrogates the ability of PACS1 to perform its normal function.

All together, our data show that de novo mutations in *PACS1* cause a hitherto unknown syndrome of ID in combination with distinct craniofacial features and genital abnormalities. The most parsimonious model is that of a dominant-negative mechanism that abrogates the ability of PACS1 to mediate the specification and migration of Sox10-positive cells in the neural crest. This in turn would perturb the migration of cells along the branchial arch, contributing to the striking craniofacial phenotype of our affected individuals. Our findings potentially implicate a splice isoform of TRPV4 in this process; however, the function of this isoform is not known, nor can we exclude that the mutation in the affected individuals also affects other PACS1 roles. Our findings highlight how the combination of detailed clinical phenotyping, unbiased genomic analysis, and

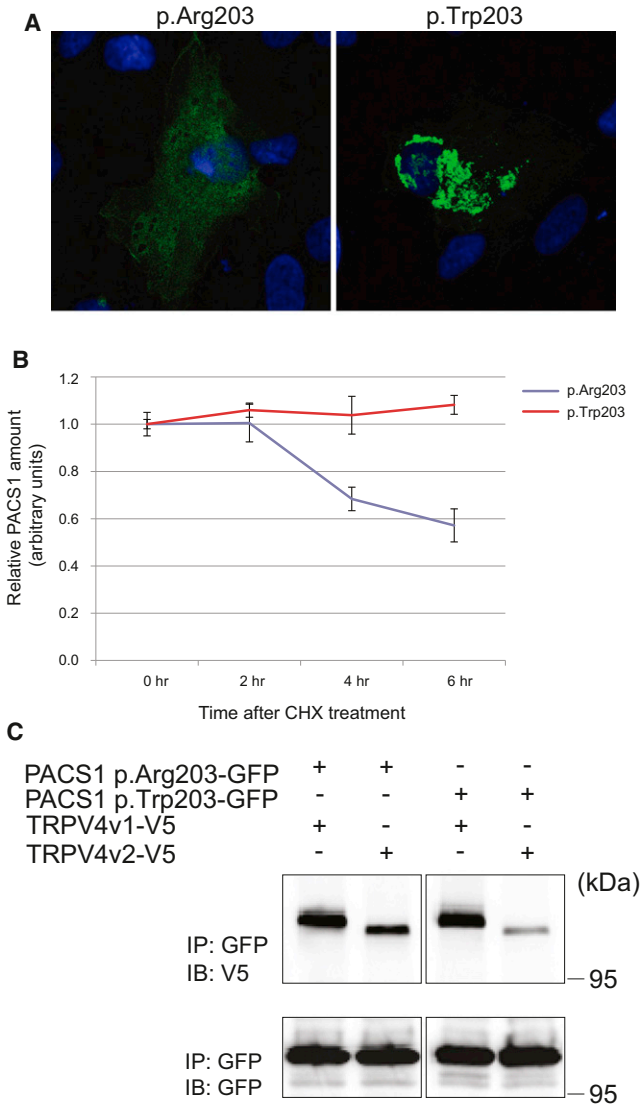

Figure 3. In Vitro Functional Characterization of the p.Arg203Trp Substitution in PACS1

(A) Localization of GFP-tagged wild-type and altered PACS1 in transfected ARPE-19 cells grown to confluence and stained with a GFP antibody. ARPE-19 cells were grown in Dulbecco's Modified Eagle Medium and Ham's F-12 Nutrient 1:1 mixture (DMEM/F-12, Invitrogen) with 10% fetal bovine serum (FBS) and 2 mM L-glutamine. Transfection of wild-type and mutant *PACS1* plasmids was carried out with FuGene6 Transfection Reagent (Roche). Cells were fixed with 4% paraformaldehyde 72 hr after transfection and were probed with a GFP antibody (Santa Cruz, sc-8334) and a secondary antibody, Alexa Fluor 488 IgG (Invitrogen).

(B) Quantification of wild-type and p.Trp203 PACS1 stability in transfected cells treated with cycloheximide (CHX). The mean measurement of triplicate experiments is shown, and the error bar represents the SEM. HEK 293FT cells were grown in Dulbecco's Modified Eagle Medium (DMEM, Invitrogen) containing 10% FBS (Invitrogen) and 2 mM L-glutamine (Invitrogen). Cells were treated with 50 mM CHX (Sigma) for 6 hr and harvested in co-IP buffer.

(C) Immunoprecipitation of GFP-tagged wild-type and altered PACS1 and V5-tagged TRPV4v1 (RefSeq NM_021625) and TRPV4v2 (RefSeq NM_147204). HEK 293 cells were transfected with tagged constructs and harvested in co-IP buffer after 48 hr. Immunoprecipitation was performed with a GFP antibody and immunoblotted with a V5 antibody.

functional dissection of variants informs diagnosis and provides insight into fundamental biological processes such as the migration of CNCCs.

Supplemental Data

Supplemental Data include four figures and two tables and can be found with this article online at http://www.cell.com/AJHG.

Acknowledgments

We are grateful to individuals 1 and 2 and their families for their support and cooperation. We thank J. de Ligt for bioinformatics support and data analysis. This work was funded in part by National Institutes of Health grants DK072301 and MH-084018 (to N.K.), the Dutch Organization for Health Research and Development (ZON-MW grants 916-86-016 to L.E.L.M.V., 917-86-319 to B.B.A.d.V., and 911-08-025 to J.A.V.), the European-Union-funded TECHGENE project (Health-F5-2009-223143 to J.A.V.), the GENCODYS project (EU-7th-2010-241995 to H.v.B. and B.B.A.d.V.), and the Dutch Brain Foundation (2010(1)-30 to A.P.M.d.B. and 2009(1)-22 to B.B.A.d.V.). N.K. is a Distinguished Brumley Professor.

Received: July 3, 2012
Revised: September 5, 2012
Accepted: October 4, 2012
Published online: November 15, 2012

Web Resources

The URLs for data presented herein are as follows:

BrainSpan: Atlas of the Developing Human Brain, http://www.brainspan.org/

NHLBI Exome Variant Server Exome Sequencing Project, http://evs.gs.washington.edu/EVS

Online Mendelian Inheritance in Man (OMIM), http://www.omim.org

References

1. van Bokhoven, H. (2011). Genetic and epigenetic networks in intellectual disabilities. Annu. Rev. Genet. *45*, 81–104.
2. Vissers, L.E., de Ligt, J., Gilissen, C., Janssen, I., Steehouwer, M., de Vries, P., van Lier, B., Arts, P., Wieskamp, N., del Rosario, M., et al. (2010). A de novo paradigm for mental retardation. Nat. Genet. *42*, 1109–1112.
3. Simmen, T., Aslan, J.E., Blagoveshchenskaya, A.D., Thomas, L., Wan, L., Xiang, Y., Feliciangeli, S.F., Hung, C.H., Crump, C.M., and Thomas, G. (2005). PACS-2 controls endoplasmic reticulum-mitochondria communication and Bid-mediated apoptosis. EMBO J. *24*, 717–729.
4. Youker, R.T., Shinde, U., Day, R., and Thomas, G. (2009). At the crossroads of homoeostasis and disease: Roles of the PACS proteins in membrane traffic and apoptosis. Biochem. J. *421*, 1–15.
5. Schermer, B., Höpker, K., Omran, H., Ghenoiu, C., Fliegauf, M., Fekete, A., Horvath, J., Köttgen, M., Hackl, M., Zschiedrich, S., et al. (2005). Phosphorylation by casein kinase 2 induces PACS-1 binding of nephrocystin and targeting to cilia. EMBO J. *24*, 4415–4424.

6. Wan, L., Molloy, S.S., Thomas, L., Liu, G., Xiang, Y., Rybak, S.L., and Thomas, G. (1998). PACS-1 defines a novel gene family of cytosolic sorting proteins required for trans-Golgi network localization. Cell *94*, 205–216.
7. Scott, G.K., Gu, F., Crump, C.M., Thomas, L., Wan, L., Xiang, Y., and Thomas, G. (2003). The phosphorylation state of an autoregulatory domain controls PACS-1-directed protein traffic. EMBO J. *22*, 6234–6244.
8. Scott, G.K., Fei, H., Thomas, L., Medigeshi, G.R., and Thomas, G. (2006). A PACS-1, GGA3 and CK2 complex regulates CI-MPR trafficking. EMBO J. *25*, 4423–4435.
9. Cordero, D.R., Brugmann, S., Chu, Y., Bajpai, R., Jame, M., and Helms, J.A. (2011). Cranial neural crest cells on the move: Their roles in craniofacial development. Am. J. Med. Genet. A. *155A*, 270–279.
10. Sauka-Spengler, T., and Bronner-Fraser, M. (2008). A gene regulatory network orchestrates neural crest formation. Nat. Rev. Mol. Cell Biol. *9*, 557–568.
11. Vaglia, J.L., and Hall, B.K. (1999). Regulation of neural crest cell populations: Occurrence, distribution and underlying mechanisms. Int. J. Dev. Biol. *43*, 95–110.
12. Fiorio Pla, A., Ong, H.L., Cheng, K.T., Brossa, A., Bussolati, B., Lockwich, T., Paria, B., Munaron, L., and Ambudkar, I.S. (2012). TRPV4 mediates tumor-derived endothelial cell migration via arachidonic acid-activated actin remodeling. Oncogene *31*, 200–212.
13. Holzer, P. (2011). Transient receptor potential (TRP) channels as drug targets for diseases of the digestive system. Pharmacol. Ther. *131*, 142–170.
14. Shin, S.H., Lee, E.J., Hyun, S., Chun, J., Kim, Y., and Kang, S.S. (2012). Phosphorylation on the Ser 824 residue of TRPV4 prefers to bind with F-actin than with microtubules to expand the cell surface area. Cell. Signal. *24*, 641–651.
15. Ahmed, M.K., Takumida, M., Ishibashi, T., Hamamoto, T., and Hirakawa, K. (2009). Expression of transient receptor potential vanilloid (TRPV) families 1, 2, 3 and 4 in the mouse olfactory epithelium. Rhinology *47*, 242–247.
16. Jenkins, P.M., Zhang, L., Thomas, G., and Martens, J.R. (2009). PACS-1 mediates phosphorylation-dependent ciliary trafficking of the cyclic-nucleotide-gated channel in olfactory sensory neurons. J. Neurosci. *29*, 10541–10551.
17. Liedtke, W., Tobin, D.M., Bargmann, C.I., and Friedman, J.M. (2003). Mammalian TRPV4 (VR-OAC) directs behavioral responses to osmotic and mechanical stimuli in Caenorhabditis elegans. Proc. Natl. Acad. Sci. USA *100*(*Suppl 2*), 14531–14536.